Interplay among Sequence, Folding Propensity, and Bio-Piezoelectric Response in Short Peptides and Peptoids

Christopher W. Marvin,[‡] Haley M. Grimm,[‡] Nathaniel C. Miller, W. Seth Horne, and Geoffrey R. Hutchison**

Department of Chemistry, University of Pittsburgh, 219 Parkman Avenue, Pittsburgh, Pennsylvania 15260.

AUTHOR INFORMATION

Corresponding Author

*horne@pitt.edu; *geoffh@pitt.edu

ABSTRACT: Many biomaterials are piezoelectric (i.e., mechanically deform under an applied electric field); however, the molecular origin of this phenomenon remains unclear. In the case of protein-based scaffolds, one possibility involves flexible response of local folding motifs to the applied field. Here, we test this hypothesis by examining piezo response in a series of helical peptide-based oligomers. Control over folding propensity is exerted through systematic variation in both side-chain sequence and backbone composition. Piezo response is quantified by piezo force microscopy on polar self-assembled monolayers. The results indicate backbone rigidity is an important determinant in peptide electromechanical responsiveness.

TOC GRAPHIC

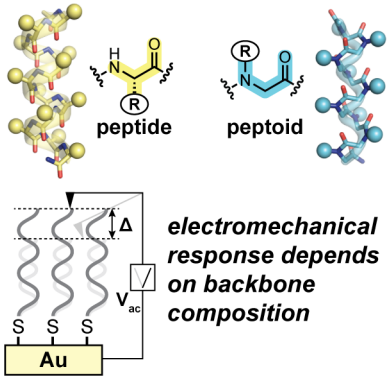

Introduction

Piezoelectric materials interconvert between electrical and mechanical energy, generating electric charge in response to mechanical stress (the direct piezoelectric effect) and undergoing deformation under an applied field (the converse piezoelectric effect).[1] Because piezoelectric materials allow direct mechanical to electrical conversion, they find wide use in touch and force sensors,[2] microscale actuators,[3] and related components. Devices utilizing such components have applications in areas from consumer to medical to military.[4,5]

Many bulk inorganic materials are piezoelectric, including lead zirconate titanate (PZT) perovskites,[6] zinc oxide,[7] and quartz.[8] Piezo response has also been shown in organic polymers such as polyvinylidene difluoride (PVDF).[9] While most applications have focused on the above materials due to their high responsiveness, the piezoelectric effect is a common molecular property[10] and is found in a number of biomaterials. As an example, proteins and their assemblies can show dramatic motion in response to environmental changes (e.g., redox, pH, chemical gradient), and this characteristic extends to applied electric fields. Prior work has shown the piezoelectric effect in collagen,[11,12] viruses,[13] aligned peptide crystals,[14,15] isolated peptide nanotubes,[16] as well as fibrils based on α-helices.[17]

Despite widespread potential applications, limitations exist that hinder the advance of piezoelectric materials. From a practical standpoint, there is an unmet need for biocompatible materials that possess strong, stable piezo-coefficients and can be scaled to fit small devices. From a fundamental perspective, there are open questions as to what molecular properties give rise to a strong piezoelectric response. These issues are interrelated. Enhanced understanding of the mechanisms giving rise to piezo response will enable the bottom-up design of new systems that address practical needs.[18]

To gain insight into the molecular basis for electromechanical response in organic scaffolds, we have previously applied computational methods to probe the piezo effect of individual molecules[10] and hydrogen-bonded assemblies.[19,20] These results suggest that the two key features necessary for piezo response at the molecular level are (1) a dipole moment to couple to the applied electric field and (2) a deformable conformation along a low energy vibrational mode. Using standard solution self-assembly techniques, one can easily create monolayers with intrinsic polar order to screen molecules for the above properties (Figure 1A).[21] As a proof of concept for the above method, we recently demonstrated piezo response in simple oligo-alanine peptide monolayers.[21] Comparison of the oligo-alanine peptide monolayer to simple alkane monolayers indicated the conformational flexibility of the polypeptide backbone was essential for piezo response.[21] Not clear was the potential role of peptide folding in this effect. One possibility is that the α-helix (Figure 1B), likely favored in the Ala-rich sequence, can act as a polar "molecular spring" that undergoes conformational deformation in an applied field. If true, this would imply a correlation between peptide helicity and the magnitude of piezo response. Here, we systematically probe the interplay among peptide chemical structure, folding propensity, and piezoelectric properties, uncovering in the process new insights into the origin of peptide electromechanical response.

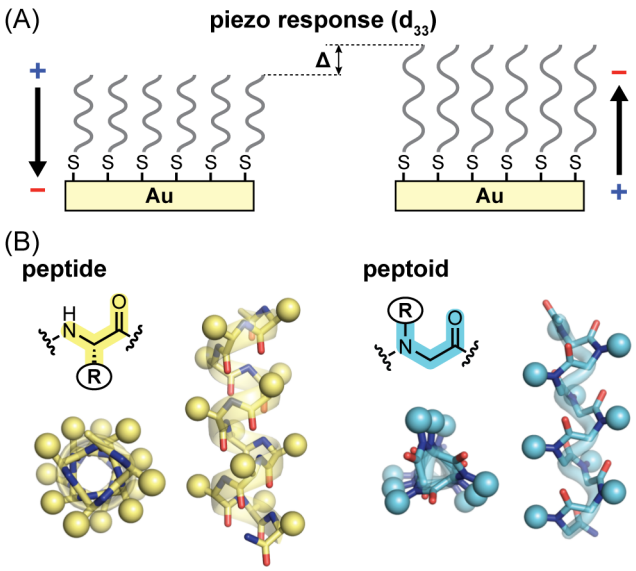

Figure 1. (A) Simplified schematic depicting nanoscale piezo response of a self-assembled monolayer on gold upon applying an electric field. (B) Backbone chemical structures alongside models of the α-helix and PPI-helix folds formed by peptide and peptoid oligomers, respectively.

To evaluate the effect of helicity, and thus the molecular basis of peptide piezoresponse, we designed a series of peptides (**1**-**3**) of identical length but varying folding propensity (Figure 2). Keeping the molecule size and composition similar among the series focuses the analysis of structure-function relationship on folding behavior. Peptide **1** is based on a previously reported sequence that is among the shortest known to show appreciable helical folded population in aqueous solution.[22] This characteristic results from the presence of three aminoisobutyric acid (Aib, U) residues that restrict backbone conformational freedom and promote the helical fold. We replaced the three Aib residues in **1** with either alanine (Ala, A) or glycine (Gly, G) to generate peptides **2** and **3**, respectively. Ala is also helix promoting, though to a lesser degree than Aib, while Gly is strongly helix disrupting. Each peptide was functionalized with a thiol group at the

N-terminus to provide an anchor point for attachment to gold in the fabrication of polar monolayers.

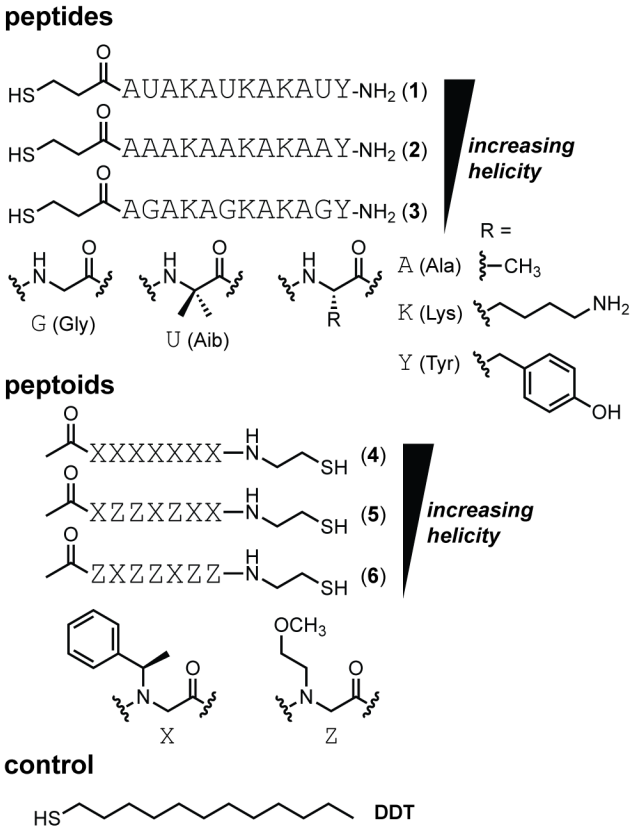

Figure 2. Peptides **1**-**3**, peptoids **4**-**6**, and control small molecule dodecanethiol (**DDT**).

A powerful strategy complementary to sequence modification for controlling folding in peptides is to alter the chemical structure of the backbone. Many backbone compositions differing from nature can give rise to discrete folding motifs.[23-26] One of the first artificial scaffolds shown to manifest such behavior is the peptoid, a variant of the α-peptide backbone where each side chain is transposed from C_α to N.[27,28] Peptoids are intrinsically more flexible than peptides; however, incorporation of α-chiral aromatic side chains such as the (*R*)-α-methylbenzyl moiety in residue X (Figure 2) gives rise to highly rigid chains that adopt polyproline-I (PPI) helical folds.[27]

Following logic analogous to that applied in peptides **1**-**3**, we designed a series of peptoids (**4**-**6**) of identical length but systematically altered helicity by combining known structure-promoting (X) and structure-disrupting (Z) residues in varying fractions.[29,30] The macrodipole of the PPI helix (δ+ toward C-terminus) is oriented opposite that of the α-helix (δ+ toward N-terminus). To keep the alignment of the helix dipole the same in the polar monolayers across the oligomers examined, we placed the thiol for anchoring to gold at the C-terminus in the peptoid series through incorporation of a terminal cysteamine. Density functional theory calculations indicate the macrodipole for a 12-residue peptide α-helix (54 D) is approximately double that of a 7-residue peptoid PPI helix (27 D). These values assume fully folded helical states, and the magnitude of the macrodipole will vary greatly with folded structure.

Experimental Methods

General Information. All Fmoc α-amino acids and resins used for solid phase synthesis were purchased from Novabiochem. Solvents and other reagents were purchased from Sigma-Aldrich and used without further purification. Reverse phase HPLC was carried out using Phenomenex Luna C_{18} columns. Products were eluted using gradients between 0.1% TFA in water (solvent A) and 0.1% TFA in acetonitrile (solvent B), monitored by UV detection at 220 nm and 280 nm. MALDI-TOF MS experiments were performed on a Voyager DE Pro (Applied Biosystems) or an ultrafleXtreme (Bruker) using α-cyano-4-hydroxy cinnamic acid as the ionization matrix.

Peptide Synthesis. Peptides **1**-**3** were synthesized by microwave-assisted Fmoc solid phase methods on a CEM MARS 5 microwave using NovaPEG rink amide resin (0.05 mmol scale). Resin was swelled in DMF for 15 min prior to the first coupling reaction. For a typical cycle, a 0.1 M solution of HCTU in NMP (4 equiv relative to resin, 2 mL, 0.20 mmol) was added to Fmoc-

protected amino acid (4 equiv, 0.20 mmol), followed by DIEA (6 equiv, 0.30 mmol). After a 2 min preactivation, the solution was transferred to resin, and the mixture heated to 90 °C over 1.5 min, followed by a 2 min hold at that temperature. Fmoc deprotection was carried out by treatment with 20% 4-methylpiperidine in DMF (4 mL), and the mixture was heated to 90 °C over 2 min, followed by a 2 min hold at that temperature. The resin was washed 3 times with DMF after each coupling and deprotection cycle. For Aib residues and those coupled to it, PyAOP (4 equiv, 0.20 mmol) was used in place of HCTU. The N-terminus of each peptide was capped with S-trityl-3-mercaptopropionic acid using the standard HCTU coupling described above. After the final coupling, the resin was washed 3 times each with DMF, DCM, and MeOH, and the resin was dried under vacuum for at least 20 min. Peptides were cleaved from resin by treatment with a solution of TFA/EDT/H_2O/TIS (92.5%/3%/3%/1.5% by volume) for 3 hours followed by precipitation in cold ether. The pellets were collected by centrifugation and re-dissolved in 90:10 solvent A / solvent B for purification by preparative HPLC. The identity and purity of final products were confirmed by analytical HPLC (Figure S1) and MALDI-TOF MS (Table S1). Peptide stock solution concentrations were quantified by UV spectroscopy (Hewlett Packard 8452A Diode Array Spectrometer, ε_{276} = 1450 cm^{-1} M^{-1} from the single Tyr in each sequence).

Peptoid Synthesis. Peptoids **4**-**6** were synthesized using a microwave-assisted submonomer solid phase approach on a CEM MARS 5 microwave using cysteamine 2-chlorotrityl resin (41.4 mg, 0.06 mmol). Resin was swelled in DCM for 30 min, then washed with DMF prior to the synthesis. In a typical cycle, a solution of 1.2 M bromoacetic acid in dry DMF (1.0 mL, 1.2 mmol) was added to resin, followed by DIC (188 μL, 1.2 mmol). The reaction was heated to 35 °C over 2 min, followed by a 2 min hold at that temperature. The resin was washed three times with DMF, followed by addition of a 1.5 M solution of primary amine (*R*-(+)-α-methylbenzylamine or 2-

methoxyethylamine) in NMP (1.6 mL, 2.4 mmol). The mixture was then heated to 90 °C over 2 min, followed by a 2 min hold at that temperature. The resin was washed again with DMF (3x) prior to the next cycle. The N-terminus of each peptoid was capped by treatment of resin with a solution of DMF (800 μl), DIEA (200 μl), and acetic anhydride (100 μl) and stirring at ambient temperature for 20 min. The resin was then washed 3 times each with DMF, DCM, and MeOH, and dried under vacuum for at least 20 min. Each peptoid was cleaved from resin by treatment with a mixture of TFA/H_2O/TIS (95%:2.5%:2.5% by volume) for 30 min. The cleaved peptoid solution was diluted in H_2O, lyophilized, and re-dissolved in 50:50 solvent A / solvent B for purification by preparative HPLC. The identity and purity of final products were confirmed by analytical HPLC (Figure S1) and MALDI-TOF MS (Table S1). Peptoid stock concentrations were determined by weight followed by dilution to a desired concentration.

Circular Dichroism (CD). CD measurements were performed on an Olis DSM17 circular dichroism spectrophotometer. Scans were performed at 20 °C from 200-260 nm with 1 nm increments, a bandwidth of 2 nm, and a 5 sec integration time. Cells with a 2 mm path length were used. Peptide solutions (50 μM as determined by UV absorbance) were prepared in 10 mM phosphate buffer (pH 7.2). Peptoid solutions (50 μM as determined by accurate weighing) were prepared in acetonitrile (HPLC grade). Percent helical population for peptides **1**-**3** was calculated using a previously described method[22] that uses the assumption that the population only consists of two states, helical and random coil, and that the contribution to ellipticity from the random coil population is negligible at 222 nm. Fraction helical population was estimated by dividing the observed ellipticity at 222 nm, $[\theta_{obsH}]_{222}$, in deg cm^2 dmol^{-1} by the limiting value for ellipticity for a 100% helical backbone. The latter was calculated via the equation $[\theta_H]_{222} = 43000(1-[x/n])$, where n is the number of residues and x is a factor that accounts for end effects, for which a value of 2.5

was used. Percent helical population for peptoids **4**-**6** was estimated following a published method.[30]

Self-Assembled Monolayer Formation. Gold-thiol self-assembled monolayers (SAMs) were prepared using 1.0 mM dodecanethiol in ethanol, 1.0 mM peptide in distilled water, or 1.0 mM peptoid in acetonitrile. These solvents were chosen due to solubility of the molecule being deposited and have no impact on the production of the monolayers. Substrates consisted of gold metal deposited on glass (Thermo Scientific BioGold substrates produced by Electron Microscopy Sciences). Prior to SAM formation, substrates were cleaned by washing with ethanol and water, followed by sonication for 10 min in the corresponding solvent used for deposition (ethanol for **DDT**, water for **1**-**3**, acetonitrile for **4**-**6**). After cleaning, the substrates were dried with compressed air or N_2 and submerged into the solution of thiol ligand for 24 h at room temperature. The substrates were then taken out of the solution, rinsed three times with the respective solvent, blown dry, covered with aluminum foil, and placed in a desiccator for at least 1 h prior to analysis. Samples not measured immediately were stored in a desiccator, protected from light exposure.

X-ray Photoelectron Spectroscopy (XPS). XPS measurements were collected on a Thermo Scientific ESCALAB 250XI XPS spectrometer. Peptide, peptoid, and DDT monolayers were deposited on Thermo Scientific BioGold substrates produced by Electron Microscopy Sciences. A survey spectrum was collected at a pass energy of 150 eV and a dwell time of 10 ms. Au_{4f} and N_{1s} were averaged over 50 scans with a pass energy of either 100 eV for peptides **1**-**3** or 150 eV for peptoids **4**-**6** and a dwell time of 50 ms. S_{2p} spectra were taken as an average of 100 scans with a pass energy of either 100 eV for peptides **1**-**3** or 150 eV for peptoids **4**-**6** and dwell time of 50 ms. Standard baseline subtraction, normalization, and peak fits were performed. The surface density and film thickness of each SAM was estimated using a previously published method,[31] where ratio

of the sulfur and gold peak maxima, at 162 eV and 84 eV respectively, were averaged across three different spots on a single SAM to estimate the surface density. Similarly, the film thickness is estimated using the ratio of the carbon, at 284.8 eV, and gold peak maxima. The average peak ratio for a given SAM was compared to that of the measured DDT SAMs. DDT has a known packing density of 4.62×10^{14} molecules per cm^2 and a film thickness of 1.5 nm, which allows the surface density and film thickness of each monolayer to be estimated by comparison.

Atomic Force Microscopy (AFM) and Piezo Force Microscopy (PFM). AFM and PFM measurements were performed using an Asylum Research MFP-3D SPM. PFM experiments were carried out using the dual-AC resonance tracing (DART-PFM) mode. Asyelec.01-R2 (Asylum Research) iridium-coated, conductive silicon probes were used for the characterization of the surface. These tips have a free-air resonance frequency of 70 kHz, but a contact resonance of ~280 kHz. The low spring constant of 2.8 N/m was used due to the soft nature of the organic and biomaterial monolayers. Multiple tip-sample voltages from 1.5 - 4.5 V were applied for each sample, as described below. The deflection was set to -0.30 and the humidity in the sample box maintained below 30%. If ambient relative humidity was above 30%, the instrument was flushed with dry nitrogen during the measurement. For each sample, a 1 μm x 1 μm area was scanned with a scan rate of 1.0 Hz. Topography, piezoresponse amplitude, and phase images were recorded. The recorded amplitudes were q-corrected to take the tip-sample resonance amplification used by DART-PFM into account. This q-correction was performed using the default analyzing software. A histogram of the q-corrected amplitude scan was generated. The median value of the distribution was plotted versus the appropriate voltage. The slope from a linear regression of this plot for the same sample measured on the same day was used to determine a single d_{33} value for a given compound. Multiple independent experiments performed for different samples and days provided

multiple d_{33} values for each compound. These values were averaged to generate the statistics reported in Table 1.

Calculation of Dipole Moment for Model Helices. Gaussian 09 revision D.01[32] was used to perform geometry optimizations using density functional theory (DFT), with the dispersion-corrected ωB97X-D functional[33] and the 6-31G(d) basis set to optimize all computed structures. Initial geometries were generated using PyMol version 1.8.4[34] with idealized backbone dihedral angles for α-helix (peptide) or PPI (peptoid) secondary structure. Computed dipole moments from DFT have been found to be highly accurate with errors in the 0.1-0.2D range.[35]

Solution Fourier Transform Infrared Spectroscopy: Spectra were collected on a Bruker Vertex-70LS FTIR that was purged with N_2 gas for at least 30 minutes prior to taking measurements. A liquid cell with CaF_2 windows and a 50 μm spacer was assembled and this empty cell was used as the reference. The cell was thoroughly cleaned with methanol and dried with N_2 before each measurement. Lyophilized peptide powder was exchanged three times by adding 5 mM HCl solution in water (1 ml x 3) and lyophilizing to remove interfering TFA salts.[36] Peptide solutions (~ 5 mg/ml in D_2O) were measured with 1000 scans, a 3 mm aperture, and a resolution of 4 cm^{-1} collected over a range of 500-4000 cm^{-1}. Raw data for each sample were collected as a transmission spectrum, corrected by subtraction of a blank (D_2O) transmission spectrum, converted to absorption, and smoothed.

Polarization-Modulated Infrared Reflection Absorption Spectroscopy (PM-IRRAS): PM-IRRAS spectra were collected on a Thermo Fisher Nicolet iS50 FTIR Spectrometer equipped with a liquid nitrogen cooled MCT-A detector. Gold-thiol self-assembled monolayers were prepared as described above. PM-IRRAS spectra were collected with a 30 min acquisition time (3000 scans) and a resolution of 4 cm^{-1} at an incidence angle of 80°. The wavelength was centered at 1600 cm^{-}

[1] to get good signal in the amide region. Atmospheric correction was applied to all spectra, followed by a manual baseline correction, conversion to absorption, and smoothing.

Results and Discussion

Peptides **1**-**3** and peptoids **4**-**6** were prepared by standard solid-phase methods (Fmoc strategy for the peptides, submonomer approach for the peptoids). Each oligomer was purified by preparative reverse phase HPLC, and the identity and purity of the final products were confirmed by analytical HPLC and MALDI-TOF mass spectrometry.

To establish that relative solution folding propensity in **1**-**6** followed the intended trends, we used circular dichroism (CD) spectroscopy (Figure 3). Solvent conditions for CD measurements were selected based on the solutions used for monolayer preparation (aqueous for the peptides, acetonitrile for the peptoids). The CD spectrum of peptide **1** showed minima at 222 and ~208 nm, characteristic of right-handed helical secondary structure. Moving through the series **1**-**3**, the band at 222 nm decreased in magnitude and the lower wavelength signal blue shifted to ~200 nm. These changes are both diagnostic of an increase in random coil character and support our design hypothesis regarding the relative helicity across the series (**1** > **2** > **3**). Qualitative features of the CD spectra of the peptoids were consistent with the expected left-handed PPI helical fold.[29] The decrease in the intensity of the band at 222 nm with increasing fraction of flexible Z residues supported the relative trend in helical character **4** > **5** > **6**. On an absolute scale, estimated folded populations (Table 1) vary from 3% for the least helical peptide (**3**) to ~100% for the most helical peptoid (**4**).

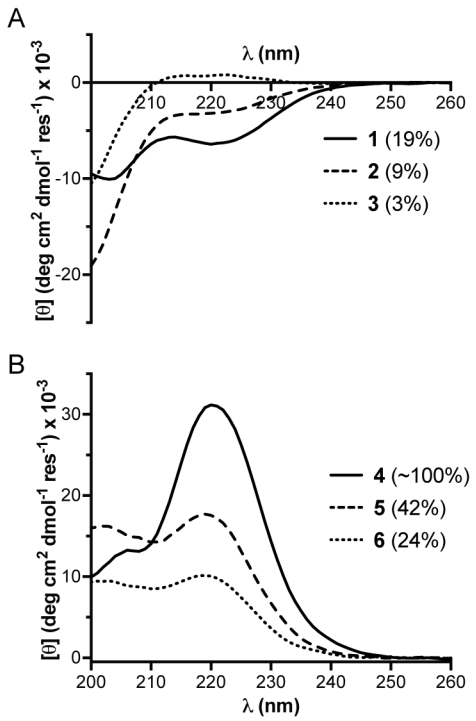

Figure 3. CD spectra of peptides **1**-**3** (50 μM in 10 mM phosphate pH 7.2) and peptoids **4**-**6** (50 μM in acetonitrile). Estimated helical folded population for each compound is indicated in parentheses.

To compare the electromechanical response of the peptides and peptoids, monolayer films were deposited by solution self-assembly on gold substrates. Using dual AC resonance tracking piezoresponse force microscopy (DART-PFM), we determined the change in thickness (Δt) of each film over a series of applied voltages (1.5 to 4 V) averaged across a 1 μm^2 area. The slope from a linear fit to a plot of Δt vs. applied voltage provides a measure of the piezoelectric response along the polarization axis (d_{33}). Ideally, the intercept of this line would pass through zero (i.e., no mechanical response with no applied field); however, due to electrostatic and tip-sample interactions, that is rarely the case. We repeated this experiment for each oligomer across independently prepared films on multiple days using different tips (Figure 4, Table 1). Averaging across multiple samples and tips minimizes artifacts arising from tip-surface interactions, and

averaging across a large area (rather than a single point) for each measurement samples an ensemble of different molecular conformations and monolayer packing motifs. The validity of the methodology was supported by the determination of the piezo response of quartz by the same approach, yielding a d_{33} (3.8 pm V^{-1}) close to the known value for d_{11} (2.3 pm V^{-1}).[8] We note that in general, across all monolayers of **1-6**, the distribution of piezo response showed high positive skewness, which did not have a clear trend with voltage. On the other hand, for five out of six compounds (**1-3**, **4**, and **6**) the distributions yielded voltage-dependent increases in peak width and standard deviation. For peptoid **5**, three out of four samples showed slight broadening with increasing voltage.

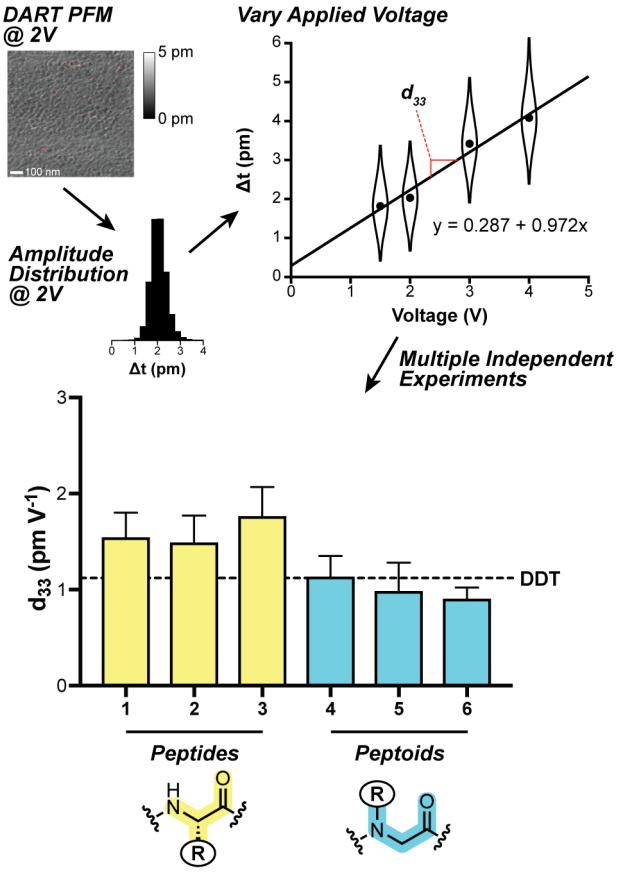

Figure 4. Summary of DART-PFM methodology used to determine piezoelectric response (see Supporting Information for details) and the resulting d_{33} values obtained from replicate

independent experiments with peptides **1**-**3**, peptoids **4-6**, dodecanethiol (**DDT**), and quartz. Error bars are the SEM from 4-8 independent experiments (see Table 1).

Table 1. Solution folding and monolayer properties for peptides **1**-**3** and peptoids **4**-**6**.

	Monolayer properties				
compound	d_{33} (pm V^{-1})[a]	*n*[a]	density (molecules cm^{-2} x 10^{14})[b]	thickness (nm)[b]	Fraction helical (%)[c]
1	1.53 ± 0.27	8	3.3 ± 0.4	2.34 ± 0.06	19
2	1.48 ± 0.29	6	4.0 ± 0.4	2.03 ± 0.08	9
3	1.75 ± 0.32	6	3.9 ± 0.4	2.56 ± 0.06	3
4	1.12 ± 0.23	4	4.1 ± 0.1	2.52 ± 0.02	100
5	0.97 ± 0.31	4	4.2 ± 0.1	2.45 ± 0.03	42
6	0.89 ± 0.13	4	4.3 ± 0.2	2.58 ± 0.02	24
DDT	1.12 ± 0.25	4	4.6[d]	1.5[d]	–
quartz	3.80 ± 0.50	2	–		–

[a] Average ± SEM for piezo coefficient (d_{33}) as determined from *n* independent PFM experiments (see supporting information for details). [b] SAM density and thickness, as estimated from XPS.[31] [c] Fraction helicity in solution as estimated by CD (see text for details). [d] From ref.[31]

Comparing the two different backbone compositions, the average response from monolayers of peptides **1**-**3** was significantly greater than that of monolayers made up of **DDT** or peptoids **4**-**6** (*p* 0.016 for peptides vs peptoids). On average, peptides **1**-**3** yielded PFM response ~41% larger than **DDT** and ~59% larger than peptoids **4**-**6**. Interestingly, no statistically significant trends beyond experimental uncertainty were discernable within a given backbone (i.e., among **1**-**3** or among **4**-**6**). While one might expect both peptides **1**-**3** and peptoids **4**-**6** to yield much greater conformational flexibility than a straight-chain alkane such as **DDT**, the high packing density in the monolayers may diminish this difference. Placing these results in context of known bulk biomaterials that are piezoactive, the d_{33} of the peptide monolayers, while small, is greater than the

response of bulk collagen (0.8 pm V^{-1}),[11] bone (0.29 pm V^{-1}),[37] and wood (0.04 pm V^{-1}).[38] It is likely that the alignment and parallel arrangement of molecular dipole moments in the monolayer samples enhances piezo response. Still, the magnitudes are modest compared to crystalline piezoelectric polymers, such as PVDF (~30 pm V^{-1}),[1] molecularly-doped polyurethane foams (~150-250 pm V^{-1}),[39] or PZT ceramics (~300-500 pm V^{-1}).[6]

To rule out the possibility that differences in piezo response observed resulted from differences in monolayer packing density rather than molecular structure, we carried out X-ray photoelectron spectroscopy (XPS). We determined the ratio of XPS peak intensities for sulfur versus gold signals for representative monolayers of **1**-**6** and **DDT** (Figure S2-S3). Calibrating against a reported packing density for **DDT**,[31] we estimated the surface coverage density for the peptides and peptoids (Table 1). Variation among the observed packing densities were small and not sufficient to explain the observed differences in piezo response. Moreover, no significant trend was apparent based on backbone composition (peptides vs peptoids) or helicity in solution. We also used the XPS peak intensities for carbon versus gold signals to estimate monolayer thickness, following published methods previously applied to peptide SAMs.[31] As with monolayer density, no clear correlations were observed to folding propensity or backbone composition (Table 1), although the value for peptide **2** was somewhat lower than the rest of the series. For peptides **1**-**3**, molecular length would be 1.8 nm for a fully α-helical fold and 4.1 nm for a fully extended conformation. For peptoids **4**-**6**, molecular length would be 1.7 nm for a fully folded PPI-helix and 3.1 nm for a fully extended chain. Thus, the observed film thicknesses (~2-2.5 nm) argue against the possibility that the chains are lying flat on the surface but also suggest the monolayer is more complex than an idealized picture of helices uniformly perpendicular to the surface. The XPS spectral characteristics also

provide evidence for the chemical integrity of the peptide and peptoid monolayers, confirming that sulfur-gold linkages were not oxidized over the course of sample preparation and storage.

In an effort to gain information about folding by an analytical method applicable both in solution SAM contexts, we turned to infrared spectroscopy. In solution FTIR spectra of peptides **1**-**3** acquired in D_2O (Figure 5A), the amide I band shifts from ~1639 to ~1645 cm^{-1} across the series. This observation is consistent with 3_{10}-helical secondary structure shifting toward increasing random coil[40,41] and matches the trend observed by CD. Polarization modulation infrared reflection absorption spectroscopy (PM-IRRAS) of the peptide monolayers showed amide I bands for peptides **1** and **2** ~1667 cm^{-1} (Figure 5B). Such spectral features have been interpreted for peptide SAMs to correspond to α-helical or distorted α-helical secondary structure.[42,43] The amide I band of peptide **3** appears at a significantly higher frequency, ~1674 cm^{-1}, which may reflect increased random coil character. An important caveat in the above analysis is that the complexity and broadness of the amide I region for all the peptide monolayers indicates a highly heterogeneous ensemble of folded states present at the surface.

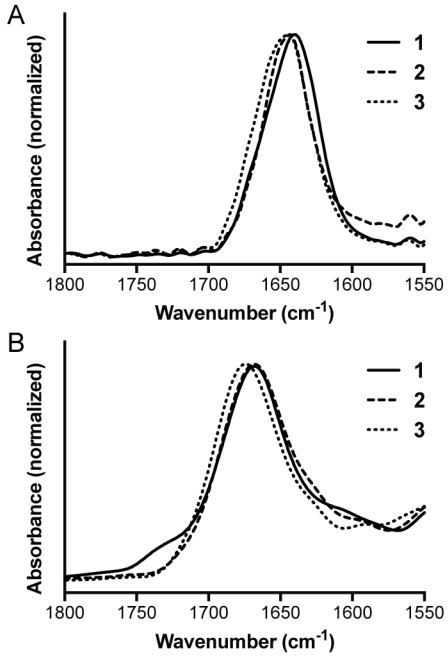

Figure 5. Amide I region from (A) solution FTIR spectra of peptides **1**-**3** (5 mg/mL in D_2O) and (B) PM-IRRAS spectra of peptide monolayers on gold.

Conclusions

In summary, the results suggest that peptide-based materials exhibiting piezo response have regions of highly polar, flexible backbones. Our initial hypothesis on the molecular basis for piezoelectric response focused on the effect of helical conformational preferences and the magnitude of the piezo response. That is, as "molecular springs," an unstructured peptide **3** would show low response. The data here argue the opposite is true and that a balance between helicity and flexibility is needed for increased molecular piezoelectric response. Small changes in helical secondary structure between peptides **1-3** results in no statistical difference in measured piezo response; however, more folded peptoids **4-6** show significantly lower response, on par with the control **DDT** alkane thiol monolayer. Structural heterogeneity in the peptide conformational

ensemble observed at the surface precludes us from saying whether a particular subpopulation of folded states in the monolayer contributes disproportionately to the observed apparent d_{33}. This open question is an important area for future study. Nevertheless, the results reported here demonstrate the promise of combining systematic synthesis, PFM monolayer characterization, and computational design in peptides and related oligomers as a means to unlock new avenues to highly responsive piezomaterials.

ASSOCIATED CONTENT

Supporting Information. The Supporting Information, including MALDI-TOF and HPLC characterization data for purified peptides and peptoids, representative XPS spectra of all species, and representative AFM and DART PFM images of all species at multiple voltages, is available free of charge on the ACS Publications website at DOI: ##

AUTHOR INFORMATION

Author Contributions

‡These authors contributed equally.

Notes

The authors declare no competing financial interests.

ACKNOWLEDGMENT

Funding for this work was provided by the National Science Foundation (DMR-1608725 to W.S.H. and G.R.H.; support for MALDI-TOF MS instrumentation through CHE-1625002).

REFERENCES

(1) Bowen, C. R.; Kim, H. A.; Weaver, P. M.; Dunn, S., Piezoelectric and Ferroelectric Materials and Structures for Energy Harvesting Applications. *Energy Environ. Sci.* **2014,** *7*, 25-44.

(2) Dahiya, R. S.; Metta, G.; Valle, M.; Adami, A.; Lorenzelli, L., Piezoelectric Oxide Semiconductor Field Effect Transistor Touch Sensing Devices. *Appl. Phys. Lett.* **2009,** *95*, 034105.

(3) Ciubotariu, D. A.; Ivan, I. A.; Clévy, C.; Lutz, P., Piezoelectric 3D Actuator for Micro-Manipulation Based on [011]-Poled PMN-PT Single Crystal. *Sens. Actuators A: Phys.* **2016,** *252*, 242-252.

(4) Ilyas, M. A.; Swingler, J., Towards a Prototype Module for Piezoelectric Energy Harvesting from Raindrop Impacts. *Energy* **2017,** *125*, 716-725.

(5) Ishikawa, M.; Uchida, Y.; Tabaru, M.; Kurosawa, M.; Kosuge, N.; Sugiyama, H., High Frequency and High Intensity Ultrasonic Transducers for Medical Applications Using Oriented Piezoelectric Thick Films by Hydrothermal Method. *J. Acoust. Soc. Am.* **2016,** *140*, 3374-3374.

(6) Lefki, K.; Dormans, G. J. M., Measurement of Piezoelectric Coefficients of Ferroelectric Thin Films. *J. Appl. Phys.* **1994,** *76*, 1764-1767.

(7) Hutson, A. R., Piezoelectricity and Conductivity in ZnO and CdS. *Phys. Rev. Lett.* **1960,** *4*, 505-507.

(8) Bottom, V. E., Measurement of the Piezoelectric Coefficient of Quartz Using the Fabry-Perot Dilatometer. *J. Appl. Phys.* **1970,** *41*, 3941-3944.

(9) Heiji, K., The Piezoelectricity of Poly (Vinylidene Fluoride). *Jpn. J. Appl. Phys.* **1969,** *8*, 975.

(10) Quan, X.; Marvin, C. W.; Seebald, L.; Hutchison, G. R., Single-Molecule Piezoelectric Deformation: Rational Design from First-Principles Calculations. *J. Phys. Chem. C* **2013,** *117*, 16783-16790.

(11) Eiichi, F.; Iwao, Y., Piezoelectric Effects in Collagen. *Jpn. J. Appl. Phys.* **1964,** *3*, 117.

(12) Anderson, J. C.; Eriksson, C., Electrical Properties of Wet Collagen. *Nature* **1968,** *218*, 166-168.

(13) Lee, B. Y.; Zhang, J.; Zueger, C.; Chung, W.-J.; Yoo, S. Y.; Wang, E.; Meyer, J.; Ramesh, R.; Lee, S.-W., Virus-Based Piezoelectric Energy Generation. *Nat. Nanotechnol.* **2012,** *7*, 351-356.

(14) Nguyen, V.; Jenkins, K.; Yang, R., Epitaxial Growth of Vertically Aligned Piezoelectric Diphenylalanine Peptide Microrods with Uniform Polarization. *Nano Energy* **2015,** *17*, 323-329.

(15) Nguyen, V.; Zhu, R.; Jenkins, K.; Yang, R., Self-Assembly of Diphenylalanine Peptide with Controlled Polarization for Power Generation. *Nat. Commun.* **2016,** *7*, 13566.

(16) Kholkin, A.; Amdursky, N.; Bdikin, I.; Gazit, E.; Rosenman, G., Strong Piezoelectricity in Bioinspired Peptide Nanotubes. *ACS Nano* **2010,** *4*, 610-614.

(17) Farrar, D.; Ren, K.; Cheng, D.; Kim, S.; Moon, W.; Wilson, W. L.; West, J. E.; Yu, S. M., Permanent Polarity and Piezoelectricity of Electrospun α-Helical Poly(α-Amino Acid) Fibers. *Adv. Mater.* **2011,** *23*, 3954-3958.

(18) Dagdeviren, C.; Yang, B. D.; Su, Y.; Tran, P. L.; Joe, P.; Anderson, E.; Xia, J.; Doraiswamy, V.; Dehdashti, B.; Feng, X.; Lu, B.; Poston, R.; Khalpey, Z.; Ghaffari, R.; Huang, Y.; Slepian, M. J.; Rogers, J. A., Conformal Piezoelectric Energy Harvesting and Storage From Motions of the Heart, Lung, and Diaphragm. *Proc. Natl. Acad. Sci. USA* **2014,** *111*, 1927-1932.

(19) Werling, K. A.; Hutchison, G. R.; Lambrecht, D. S., Piezoelectric Effects of Applied Electric Fields on Hydrogen-Bond Interactions: First-Principles Electronic Structure Investigation of Weak Electrostatic Interactions. *J. Phys. Chem. Lett.* **2013,** *4*, 1365-1370.

(20) Werling, K. A.; Griffin, M.; Hutchison, G. R.; Lambrecht, D. S., Piezoelectric Hydrogen Bonding: Computational Screening for a Design Rationale. *J. Phys. Chem. A* **2014,** *118*, 7404-7410.

(21) Quan, X.; Madura, J. D.; Hutchison, G. R., Self-Assembled Monolayer Piezoelectrics: Electric-Field Driven Conformational Changes. *submitted*.

(22) Banerjee, R.; Chattopadhyay, S.; Basu, G., Conformational Preferences of a Short Aib/Ala-Based Water-Soluble Peptide as a Function of Temperature. *Proteins: Struct., Funct., Bioinf.* **2009,** *76*, 184-200.

(23) Gellman, S. H., Foldamers: A Manifesto. *Acc. Chem. Res.* **1998,** *31*, 173-180.

(24) Bautista, A. D.; Craig, C. J.; Harker, E. A.; Schepartz, A., Sophistication of Foldamer Form and Function in Vitro and in Vivo. *Curr. Opin. Chem. Biol.* **2007,** *11*, 685-692.

(25) Goodman, C. M.; Choi, S.; Shandler, S.; DeGrado, W. F., Foldamers as Versatile Frameworks for the Design and Evolution of Function. *Nat. Chem. Biol.* **2007,** *3*, 252-262.

(26) Guichard, G.; Huc, I., Synthetic Foldamers. *Chem. Commun.* **2011,** *47*, 5933-5941.

(27) Kirshenbaum, K.; Barron, A. E.; Goldsmith, R. A.; Armand, P.; Bradley, E. K.; Truong, K. T. V.; Dill, K. A.; Cohen, F. E.; Zuckermann, R. N., Sequence-Specific Polypeptoids: A Diverse Family of Heteropolymers with Stable Secondary Structure. *Proc. Natl. Acad. Sci. USA* **1998,** *95*, 4303-4308.

(28) Sun, J.; Zuckermann, R. N., Peptoid Polymers: A Highly Designable Bioinspired Material. *ACS Nano* **2013,** *7*, 4715-4732.

(29) Wu, C. W.; Sanborn, T. J.; Huang, K.; Zuckermann, R. N.; Barron, A. E., Peptoid Oligomers with α-Chiral, Aromatic Side Chains: Sequence Requirements for the Formation of Stable Peptoid Helices. *J. Am. Chem. Soc.* **2001,** *123*, 6778-6784.

(30) Shin, H.-M.; Kang, C.-M.; Yoon, M.-H.; Seo, J., Peptoid Helicity Modulation: Precise Control of Peptoid Secondary Structures via Position-Specific Placement of Chiral Monomers. *Chem. Commun.* **2014,** *50*, 4465-4468.

(31) Lu, H.; Hood, M. A.; Mauri, S.; Baio, J. E.; Bonn, M.; Munoz-Espi, R.; Weidner, T., Biomimetic Vaterite Formation at Surfaces Structurally Templated by Oligo(Glutamic Acid) Peptides. *Chem. Commun.* **2015,** *51*, 15902-15905.

(32) Frisch, M. J.; Trucks, G. W.; Schlegel, H. B.; Scuseria, G. E.; Robb, M. A.; Cheeseman, J. R.; Scalmani, G.; Barone, V.; Mennucci, B.; Petersson, G. A. et al. Gaussian 09, Revision A.02, Gaussian, Inc. Wallingford, CT, USA, 2009

(33) Chai, J.-D.; Head-Gordon, M., Long-Range Corrected Hybrid Density Functionals with Damped Atom-Atom Dispersion Corrections. *PCCP* **2008,** *10*, 6615-6620.

(34) Schrodinger, LLC, The PyMOL Molecular Graphics System, Version 1.8. 2015.

(35) Hickey, A. L.; Rowley, C. N., Benchmarking Quantum Chemical Methods for the Calculation of Molecular Dipole Moments and Polarizabilities. *J. Phys. Chem. A* **2014,** *118*, 3678-3687.

(36) Andrushchenko, V. V.; Vogel, H. J.; Prenner, E. J., Optimization of the Hydrochloric Acid Concentration Used for Trifluoroacetate Removal from Synthetic Peptides. *J. Pept. Sci.* **2007,** *13*, 37-43.

(37) Marino, A. A.; Becker, R. O.; Soderholm, S. C., Origin of the Piezoelectric Effect in Bone. *Calc. Tis. Res.* **1971,** *8*, 177-180.

(38) Fukada, E., Piezoelectricity of Wood. *J. Phys. Soc. Jpn.* **1955,** *10*, 149-154.

(39) Moody, M. J.; Marvin, C. W.; Hutchison, G. R., Molecularly-Doped Polyurethane Foams with Massive Piezoelectric Response. *J. Mater. Chem. C* **2016,** *4*, 4387-4392.

(40) Martinez, G.; Millhauser, G., FTIR Spectroscopy of Alanine-Based Peptides: Assignment of the Amide I′ Modes for Random Coil and Helix. *J. Struct. Biol.* **1995,** *114*, 23-27.

(41) Yang, H.; Yang, S.; Kong, J.; Dong, A.; Yu, S., Obtaining Information about Protein Secondary Structures in Aqueous Solution Using Fourier Transform IR Spectroscopy. *Nat. Protoc.* **2015,** *10*, 382-396.

(42) Boncheva, M.; Vogel, H., Formation of Stable Polypeptide Monolayers at Interfaces: Controlling Molecular Conformation and Orientation. *Biophys. J.* **1997,** *73*, 1056-1072.

(43) Wen, X.; Linton, R. W.; Formaggio, F.; Toniolo, C.; Samulski, E. T., Self-Assembled Monolayers of Hexapeptides on Gold: Surface Characterization and Orientation Distribution Analysis. *J. Phys. Chem. A* **2004,** *108*, 9673-9681.